Traffic 2007; **8:** 77–88
Blackwell Munksgaard

doi: 10.1111/j.1600-0854.2006.00505.x

Case Report

Patients with a Non-dysferlin Miyoshi Myopathy have a Novel Membrane Repair Defect

Jyoti K. Jaiswal[1,*], Gareth Marlow[2], Gillian Summerill[2], Ibrahim Mahjneh[3], Sebastian Mueller[2], Maria Hill[2], Katsuya Miyake[4], Hannelore Haase[5], Louise V. B. Anderson[6], Isabelle Richard[7], Sari Kiuru-Enari[8], Paul L. McNeil[4], Sanford M. Simon[1] and Rumaisa Bashir[2]

[1]*The Rockefeller University, Box 304, 1230 York Avenue, New York, NY 10021, USA*
[2]*School of Biological and Biomedical Sciences, University of Durham, Durham, UK*
[3]*Department of Neurology, University of Oulu and MHSO Hospital, Pietarsaari, Finland*
[4]*Institute of Molecular Medicine and Genetics, Medical College of Georgia, Augusta, GA 30912-2000, USA*
[5]*Max Delbruck Center for Molecular Medicine (MDC), D-13092 Berlin, Germany*
[6]*Institute of Human Genetics, International Centre for Life, Newcastle upon Tyne, UK*
[7]*Généthon, Centre National de la Recherche Scientifique UMR 8115, 1 bis rue de l'Internationale, 91000 Evry, France*
[8]*Department of Neurology, University of Helsinki, Helsinki, Finland*
**Corresponding authors: Jyoti K. Jaiswal, jaiswaj@rockefeller.edu; Rumaisa Bashir, rumaisa.bashir@durham.ac.uk*

Two autosomal recessive muscle diseases, limb girdle muscular dystrophy type 2B (LGMD2B) and Miyoshi myopathy (MM), are caused by mutations in the dysferlin gene. These mutations result in poor ability to repair cell membrane damage, which is suggested to be the cause for this disease. However, many patients who share clinical features with MM-type muscular dystrophy do not carry mutations in dysferlin gene. To understand the basis of MM that is not due to mutations in dysferlin gene, we analyzed cells from patients in one such family. In these patients, we found no defects in several potential candidates – annexin A2, caveolin-3, myoferlin and the MMD2 locus on chromosome 10p. Similar to dysferlinopathy, these cells also exhibit membrane repair defects and the severity of the defect correlated with severity of their disease. However, unlike dysferlinopathy, none of the conventional membrane repair pathways are defective in these patient cells. These results add to the existing evidence that cell membrane repair defect may be responsible for MM-type muscular dystrophy and indicate that a previously unsuspected genetic lesion that affects cell membrane repair pathway is responsible for the disease in the non-dysferlin MM patients.

Key words: enlargeosome, exocytosis, lysosome, Miyoshi myopathy, muscular dystrophy, wound repair

Received 19 May 2006; revised and accepted for publication 20 October 2006; published online 21 November 2006

Muscular dystrophy encompasses a large and diverse group of inherited muscle diseases characterized by skeletal muscle weakness and wasting (1). They have been classified by the pattern of inheritance, the clinical phenotype and the features or function of the causative gene (1,2). Among these are limb girdle muscular dystrophy type 2B (LGMD2B) and Miyoshi myopathy (MM), which share allelic heterogeneity resulting from mutations in the dysferlin gene (1–3). Both forms show autosomal recessive inheritance but present with a variable pattern of muscle weakness at the onset of the disease. In contrast to the distal muscle weakness observed in MM, LGMD2B patients suffer from predominantly proximal muscles weakness (1,2). In MM, a common early feature is the inability of the patients to stand on tiptoe due to weakness of the gastrocnemius muscles and patients show characteristic elevated levels (10-fold to 100-fold above normal) of serum creatine kinase (CK). Both LGMD2B and MM patient muscle show absence of dysferlin protein at the sarcolemma (2–6), but no apparent genotype–phenotype correlations have been identified to explain the variable pattern of muscle weakness, especially as both diseases can be caused by the same mutation (7).

Dysferlin is a membrane protein with homology to the *Caenorhabditis elegans* protein FER-1 (3,8,9). FER-1 is responsible for mediating fusion of intracellular vesicles with the spermatid plasma membrane (10). Homology and the similar predicted protein structures of dysferlin and FER-1, characterized by tandem C2 domains and a C-terminal transmembrane domain, has led to suggestions that dysferlin may also play a role in membrane fusion (8,9). The identification of dysferlin has led to the identification of the ferlin protein family and several genes that share a similar structure and encode dysferlin-related proteins. These include otoferlin (11), myoferlin (12,13) and FER1L4 (14). Of these, otoferlin is also implicated in genetic disease, and disease-causing mutations have been identified in non-syndromic deafness patients (11,15).

The muscular dystrophy linked with dysferlin mutations termed dysferlinopathy has recently been shown to be

associated with defective cell membrane repair (3,16,17). Wounding of muscle fibers from normal mice was shown to result in accumulation of dysferlin at the site of repaired membrane (16). In contrast, muscle fibers from dysferlin-deficient mice showed poor membrane resealing (16). Sarcolemmal injury is a physiological event in normal muscle, resulting from contraction-induced mechanical stress. However, in dystrophic muscle it can be a significant contributory factor leading to muscle necrosis (18). In dysferlinopathy, membrane injury appears to be an early event. Electron microscopy analysis of non-necrotic patient muscle fibers reveals plasma membrane lesions and accumulating subsarcolemmal vesicles (16,19).

The mechanisms involved in cell membrane repair require addition of membrane from internal compartments by their fusion at or near the wound site. Fusion occurs in response to entry of calcium caused by the cell membrane disruption (20,21). Synaptotagmins, which are integral membrane proteins characterized by C2 domains are thought to function as Ca^{2+} sensors in vesicle fusion (22–25). The similarity of the calcium-dependent phospholipid-binding properties of some of the dysferlin and myoferlin C2 domains with the C2A domain in the synaptotagmins has led to suggestions that the ferlins may also function as Ca^{2+} sensors to facilitate vesicle fusion (26). Indeed, it has been proposed that Ca^{2+}-dependent fusion of dysferlin-containing vesicles at the site of plasma membrane damage is responsible for the healing of sarcolemmal wound in normal muscles (3). An independent study reported that the muscles from dysferlin knockout mice are deficient in exocytosis of lysosomes (17) – a compartment whose ability to undergo Ca^{2+}-dependent exocytosis has been linked to membrane resealing (27). In muscle cells, dysferlin localizes to the T-tubules and not lysosomes (28). Thus identity of the vesicles in the dysferlin knockout mouse cells that are responsible for the poor repair of sarcolemmal membrane wounds is presently unclear. Recently, a novel vesicle called enlargeosome, characterized by the marker protein AHNAK (desmoyokin), was identified (29). This has also been shown to undergo Ca^{2+}-dependent exocytosis, aiding in increasing the surface area of the cell membrane and resealing wounded cell membrane (29). It remains to be tested if exocytosis of this vesicle is involved in repair of membrane wounds in dysferlin-deficient cells.

The ability to make a molecular diagnosis of MM-type muscular dystrophy has increased its awareness and also led to recognition that MM is genetically heterogeneous. Clinical and genetic studies of Dutch families with MM-type muscular dystrophy has highlighted that not all families with similar clinical features as dysferlin MM have mutations in the dysferlin gene (30). These studies have highlighted the existence of further MM loci, and in two unrelated Dutch families, linkage analysis studies have tentatively assigned a second MM locus (designated MMD2) to chromosome 10p [Zmax = 2.578 ($\theta = 0$) at D10S2325] (30).

In an attempt to identify the molecular basis of MM-type muscular dystrophy in patients who show normal dysferlin expression, we investigated if they have defects in MMD2 and other candidate loci such as annexin A2, caveolin-3 and myoferlin. We found no defects in any of these loci that would indicate their role in the disease in these patients. Due to the similarity in the disease phenotypes between dysferlin and non-dysferlin MM, we hypothesized that non-dysferlin MM may also be associated with inability of cells to repair damage to their plasma membrane. Here, we show that fibroblasts from these non-dysferlin MM patients are defective in membrane repair, despite being proficient in wound-induced exocytosis of lysosomes and the enlargeosomes – compartments that are suggested to be responsible for membrane repair. This study points to a novel defect in cell membrane repair and indicates that a novel genetic locus is responsible for this MM-type muscular dystrophy. It also emphasizes that inability to repair cellular wounds may be a common feature of MM-type muscular dystrophies.

Results

Clinical history and dysferlin analysis in the MM patients

Patient 1, a 41-year-old man displayed onset of the first muscle symptoms at the age of 20 as pains and burning sensations in the calves. At age 25–27 years, he began to have difficulty in running. The first clinical assessment for the muscle symptoms at age 23 years revealed the presence of highly elevated serum CK levels, 12 000–16 000 (normal are $<$290 U/L). Physical examination showed only slight weakness of calf muscles – the Medical Research Council grade of 4 out of 5 and hypertrophy of the extensor digitorum brevis (EDB) muscles. Muscle magnetic resonance imaging (MRI) scans showed moderate fatty replacement of the gastrocnemius and soleus, as well as adductor magnus (even if clinically this muscle showed normal force 5/5). The patient has been unable to run, since 30 years of age and climbs stairs with assistance since the age of 34 years but does not require walking assistance. Physical examination was repeated at age 38 years, the patient presented mild waddling gait with loss of push off movements during the two phases of the gait. There was slight lordosis and rising from the chair was possible only with support. Muscle force examination showed weakness on the ileopsoas and hamstrings (3+/5), gluteus maximum, hip adductors, gastrocnemius and soleus (3/5). There was bilateral hypertrophy of the EDB muscle. Normal reflexes were recorded and no contractures were detected. The muscle MRI scans control showed worsening of the calf muscles, fatty degeneration changes seen at the first exam and slight to moderate involvement of the left hamstring muscles.

Patient 2, a 46-year-old man, has not complained of any symptoms and appears healthy. Muscle examination at

age 44 showed normal muscle forces (5/5). Serum CK levels were high (1500 U/L). Muscle MRI scans showed gastrocnemius medial fatty degeneration slight on the right and moderate on left (even if clinically this muscle showed normal force, 5/5). From these findings, a diagnosis of MM was made. Although muscle biopsies were available for both patients, sufficient muscle proteins for immunoblot analysis were extracted only for patient 2. Immunoblot analysis revealed dysferlin levels in patient 2 is similar to control. To confirm this further, we examined dysferlin protein levels in cultured fibroblasts generated from recently acquired biopsies from affected and control patient using the NCL-Hamlet dysferlin antibody. We found that cells from both patients had strong dysferlin expression, although marginally lower than the control cells (Figure 1B, C light gray bars). To further exclude a role of dysferlin in disease in these patients, we performed haplotype analysis of the dysferlin region in this family. Haplotype analysis was performed using microsatellite markers mapping around the dysferlin gene and only data for informative markers has been presented. The haplotype data are consistent with exclusion of dysferlin (Figure 1A). Both patients have inherited different maternal chromosome 2 regions spanning the dysferlin locus from the distal marker D2S292 up to the region represented by the marker D2S291 mapping proximal to dysferlin. All the markers tested identified recombinants in the affected patients. This family was therefore excluded for dysferlin, and these patients were classified as non-dysferlin MM patients.

Genetic and biochemical analysis of candidate non-dysferlin MM loci

We examined several candidate MM loci – (i) Annexin A2 – It associates with dysferlin in a Ca^{2+}-dependent manner and is believed to be necessary for proper localization and activity of dysferlin. Western blot analysis revealed that full-length annexin A2 is abundantly expressed in both

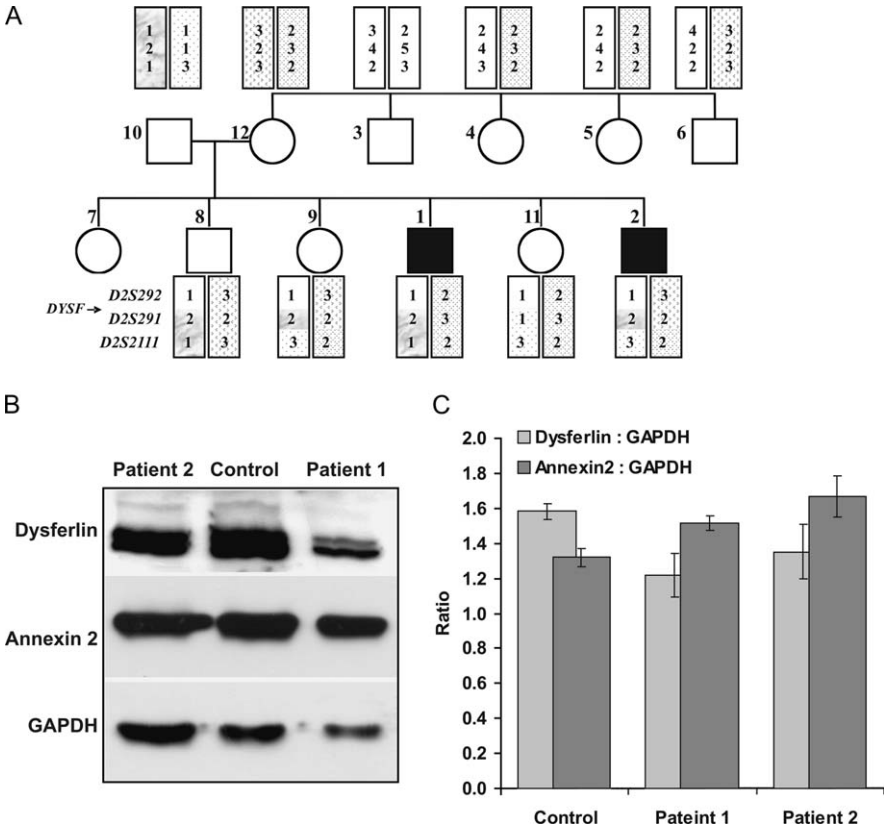

Figure 1: Analysis of dysferlin and annexin A2 in the patient cells. A) Haplotype analysis of the *DYSF* region on chromosome 2p13. The blackened symbols in the pedigree represent the affected patients. The maternal and paternal chromosomes are represented by different shading patterns and uninformative genotypes have not been shaded. Both patients have inherited different maternal chromosome 2 regions spanning the dysferlin locus from the distal marker D2S292 up to the region represented by the proximal marker D2S291. All the markers are recombinant in the affected patients, the data being consistent with exclusion to dysferlin. B) Western blot analysis of the dysferlin and annexin A2 in patient fibroblasts. The dysferlin-specific NCL-hamlet antibody detects a doublet band at 230 kDa in fibroblast cells, and the annexin A2 monoclonal antibody detects the expected single band at 35 kDa. Both proteins are abundantly expressed in the patient cells. C) The density of dysferlin and annexin A2 bands were normalized for each sample using GAPDH as the loading control. The ratio of the density of protein of interest to GAPDH is plotted here and represents the average of two experiments carried out in duplicates. The error bars show the standard deviation (SD).

patient cells to a level that is comparable to the control cells (Figure 1B, C dark gray bars). (ii) Caveolin-3 – The protein synthesized by the caveolin-3 locus interacts with dysferlin and is important for its proper trafficking (31). Caveolin-3 is deficient in muscle diseases, including LGMD1C and a distal muscular dystrophy (32). By sequencing, we detected no pathogenic mutations in either exon of caveolin-3 in each of the patient DNA samples. However, we identified two independent CAV3 polymorphisms in both affected individuals. The first polymorphism, in codon 33 changes the third base from C>T and has been reported previously (http://www.ncbi.nlm.nih.gov/sutils/evv.cgi?taxid=9606&contig=NT_022517.17&gene=CAV3). The second polymorphism is novel and is present in codon 9, also resulting in a C>T change in both affected individuals and the unrelated control. Both polymorphisms were expressed as heterozygous. (iii) The myoferlin locus produces a dysferlin-related protein showing high expression in regenerating muscle (12,33). Myoferlin-deficient muscle shows defects in myogenesis and these muscles do not regenerate as well as wild-type muscles (33). Myoferlin is also upregulated in mdx dystrophic muscle, which undergoes extensive muscle regeneration (12). We carried out Western blot analysis to monitor the expression of myoferlin protein in patient and control cells using a monoclonal antibody. As has been reported by others (34), our myoferlin monoclonal antibody also detected a 230-kDa protein in C2C12 cells (Figure 2A). To test the specificity of the antibody, C2C12 lysate immunoblots were probed with myoferlin monoclonal antibody pre-adsorbed with the myoferlin peptide used to generate the antibody. This resulted in no signal in these samples (Figure 2A). Analysis of the patient and control cell lysates using this antibody revealed that the patient and control cells have similar levels of myoferlin protein (Figure 2A). (iv) Involvement of the MMD2 region – Genetic heterogeneity in MM was first described by Linssen et al. (30). In two Dutch MM families not linked to dysferlin mutations, a microsatellite-based genome scan suggested a tentative linkage to chromosome 10p, although the linkage data just fell short of

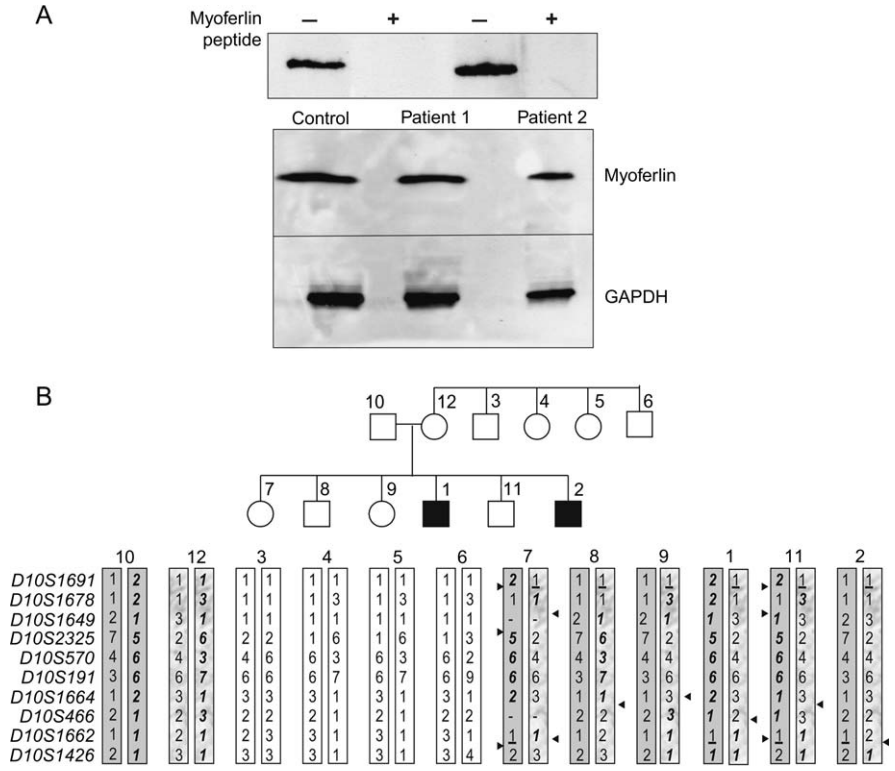

Figure 2: Analysis of the candidate genes for their involvement in non-dysferlin MM. A) Myoferlin protein expression is not altered in non-dysferlin MM patient fibroblasts. i) Immunoadsorption analysis was performed using C2C12 cell lysates to determine the specificity of the myoferlin monoclonal antibody. The monoclonal myoferlin antibody detects a 230-kDa protein in C2C12 cells. No signal was detected in C2C12 lysate immunoblots incubated with myoferlin monoclonal antibody after pre-adsorption with the myoferlin peptide used to generate the antibody. ii) Fibroblast cell lysates also express a 230-kDa myoferlin protein. No differences in myoferlin protein expression are detected between patient and control cells. B) Haplotype analysis of the chromosome 10p region to which the *MMD2* gene has been mapped. The blackened symbols in the pedigree represent the affected patients. The paternal chromosomes are represented as dark gray and the maternal chromosomes as light gray. The arrow depicts recombination points. Alleles that have been underlined are uninformative. The affected individuals 1 and 2 have inherited different paternal chromosomes 10p regions. Only the paternal genotypes for the marker D10S1662 are uninformative in the affected patients. Despite this, the affected patients have inherited different maternal D10S1662 genotypes excluding the involvement of this region for the disease.

statistical significance. We selected microsatellites covering this region, which we have assigned MMD2 and those mapping at the recombination boundaries in the affected patients. We performed haplotype analysis of 12 microsatellite markers mapping to the MMD2 locus in the family showing defective membrane repair (Figure 2B). Haplotype data for two markers were uninformative and their genotypes have not been presented. The haplotype analysis showed that affected patients 1 and 2 have inherited different paternal chromosome 10p regions, highlighting exclusion to the MMD2 region. The only marker that was not fully informative was D10S1662. Although the paternal genotype generated for D10S1662 was uninformative in the affected patients, they have inherited different maternal D10S1662 genotypes, highlighting recombination at this region. From these analyses, we excluded four candidate genes for their role in non-dysferlin MM. Moreover, exclusion to chromosome 10p to the region to which MMD2 has been tentatively linked suggests further heterogeneity in MM.

Patient cells fail to repair membrane damage

Fibroblasts are commonly used for functional studies of muscular dystrophy and have resulted in better understanding of several muscle diseases such as distal myopathy with rimmed vacuoles, muscle–eye-brain disease and Emery–Dreifuss muscular dystrophy to name a few (35–38). Moreover, dysferlin trafficking and the effect of caveolin-3 disease mutations on this process in muscle cells can be recapitulated in the fibroblasts (31). Together, these indicate that fibroblasts can be used to study the muscle cell defects in muscular dystrophy. We used fibroblast from these non-dysferlin MM patients and an unrelated control to first examine if like dysferlin-deficient cells, these cells also exhibit defect in healing membrane damage. To assess the membrane resealing ability of the non-dysferlin MM patient and control fibroblasts, two independent approaches were used. In the first method, membrane damage was induced by multiphoton laser irradiation in the presence of the fluorescent dye FM-143. The fluorescence near the disruption site was measured at 10-seconds intervals beginning 20 seconds before t0 (time of membrane wounding) and extending till 7 min later. FM-143 fluoresces brighter in a lipid environment. Thus in cells that are wounded, but not healed, the fluorescence increases as the FM-143 entering the cells binds to internal membranes. When the membrane damage is resealed, further intracellular entry of the dye is blocked and the fluorescence stops increasing. The calcium dependency of membrane resealing has been observed in many cell types, including fibroblasts (21,27). Accordingly, control and patient cells wounded in the absence of Ca^{2+} were unable to impede dye entry over the 7-min time-course for which these cells were monitored, indicating a failure to reseal (Figure 3A). In contrast, control fibroblasts wounded in the presence of Ca^{2+} impeded dye entry within a minute after membrane damage (Figure 3A), indicating that in the presence of

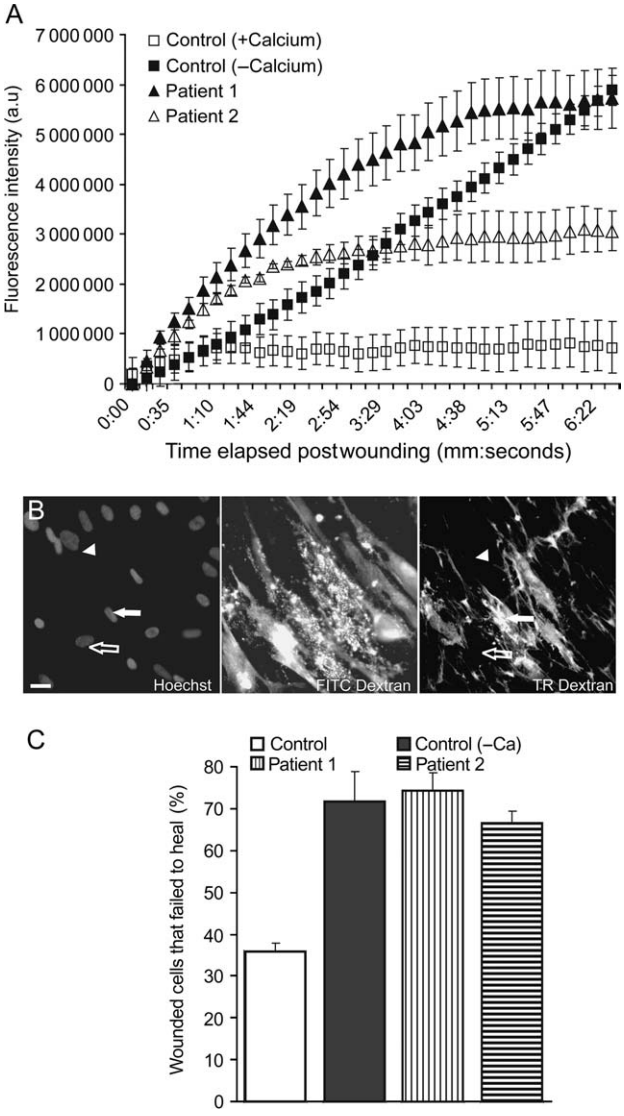

Figure 3: Patient cells are inefficient at healing plasma membrane wounds. A) Patient and control fibroblasts were wounded with pulsed two-photon laser in DPBS + 2 μM FM1-43 with 2 mM Ca^{2+} (+ calcium) or 1 mM EGTA (– calcium). The cells were imaged using 488 nm one-photon excitation at 10-seconds intervals starting from the time of wounding. The plot shows average of FM1-43 emission intensities of five cells of each type, error bars indicate SD. B) Control fibroblasts were wounded by glass beads in the presence of FITC dextran and 2 mM Ca^{2+} and then incubated in TR dextran after 5 min. The cells were fixed and nuclei labeled with Hoechst 3342. Epifluorescence images shown here were acquired using a 20× 0.7 NA objective. Arrowhead indicates an unwounded cell, open arrow indicates a cell that healed its wound prior to TR dextran addition and the filled arrow indicates a cell that failed to heal its wound resulting in loss of much of FITC dextran and strong TR dextran labeling. Scale represents 10 μm. C) Following bead wounding in the conditions described, >100 wounded cells were counted for each sample to determine cells that failed to heal their membrane damage.

Ca^{2+}, the cells reseal their damaged membranes within a minute (Figure 3A). Identical laser induced membrane disruption of patient 2 fibroblasts in the presence of Ca^{2+} impeded FM-143 dye entry starting 2 min after membrane injury, twice as long as in the control cells. This suggests that the cells of this patient were slower at resealing a disruption in their membrane. When fibroblasts from patient 1 were wounded in presence of Ca^{2+}, the dye entry was unimpeded for over 4 min (Figure 3A). This suggests that cells of patient 1 are even poorer in resealing membrane disruptions than patient 2. The differences in the resealing capability of the cells from the two patients appear to correlate with the severity of the muscular dystrophy displayed by each patient.

As an independent test of the wound-healing ability of the patient cells, we carried out glass-bead-mediated wounding in the presence of calcium. Cells were wounded in the presence of fluorescein isothiocyanate (FITC)-labeled dextran, which resulted in cytosolic labeling of all wounded cells with FITC dextran. At 5 min post-injury, the glass beads and FITC dextran were removed and replaced with Texas Red (TR) dextran. This resulted in TR labeling of only those cells that fail to heal within 3 min (Figure 3B). During the TR dextran labeling and subsequent washes, cells that failed to heal also lost much of their FITC dextran. This resulted in three populations of cells: (i) those that are not labeled, these are the unwounded cells (arrowhead); (ii) cells that have a stronger FITC dextran labeling, these are wounded cells that healed their membrane damage during the 3-min interval (open arrow); and (iii) cells that have stronger TR dextran labeling, these are cells that fail to heal their wound (filled arrow). Quantification of these three populations of cells indicates that 36 $\pm$ 2% of the control fibroblasts wounded in the presence of 2 mM extracellular Ca^{2+} failed to heal. Almost twice as many fibroblasts of patient 1 (74 $\pm$ 4%) and patient 2 (66 $\pm$ 3%) ($P = 5 \times 10^{-7}$ for each) failed to heal their membrane damage (Figure 2C). The 12% difference between the number of patient cells that failed to heal is also statistically significant ($P = 2.7 \times 10^{-2}$).

Patient cells are proficient in Ca^{2+}-dependent lysosomal exocytosis

Two independent approaches were followed to monitor the lysosomal exocytosis in these cells. In the first approach, we used total internal reflection microscopy (TIR-FM) to monitor if calcium can trigger exocytosis of individual lysosomes in real time in live cells. Lysosomes were selectively labeled with fluorescent (FITC) dextran and their ability to undergo calcium-triggered exocytosis studied by generating calcium increase with calcium-specific ionophore calcimycin (39). Using this approach, we detected calcium-triggered lysosomal exocytosis in control fibroblasts (Video S1) and fibroblasts from patient 1 (Video S2) and patient 2 (Video S3). The rate of lysosomal exocytosis, as judged by the rate of exocytosis following calcium triggering (by calcimycin), was similar between the control and patient cells (Figure 4A; $P > 0.4$).

In a complimentary approach, we monitored calcium-dependent appearance of lysosomal membrane proteins on the cell surface. Control and patient fibroblasts were treated with 10 μM calcium ionophore, and the cell surface LAMP1 was detected by using an antibody specific to the luminal domain of LAMP1, which becomes extracellular following lysosomal exocytosis. Ionophore treatment resulted in increase in LAMP1 staining on the surface of the control and both the patient cells (Figure 4B). Next, we used the same approach to test exocytosis of lysosomes following cell wounding. As described in the wound-healing assay, cells were wounded with glass beads in buffer with 2 mM Ca^{2+} and 4 mg/mL FITC dextran. Cells were allowed to heal for 5 min and then immunostained for cell surface LAMP1. Most unwounded cells showed little or no cell surface LAMP1 staining, but over two-thirds of all of wounded cells (>150) showed cell surface LAMP1 (Figure 5). There was no difference in the number of wounded cells that exocytosed lysosomes between control (85 $\pm$ 2%; $n = 157$), patient 1 (76 $\pm$ 10%; $P > 0.05$; $n = 179$) and patient 2 (74 $\pm$ 8%; $P \geq 0.05$; $n = 169$) (Figure 5A, B). However, greater number of wounded patient fibroblasts showed high cell surface LAMP1 levels compared with wounded control cells (data not shown). Thus, wounding of these patient cells induces lysosomal exocytosis that is comparable or greater than what is observed in wounded control cells.

Patient cells are proficient in Ca^{2+}-dependent enlargeosomal exocytosis

Next, we investigated enlargeosomal exocytosis, which is another pathway proposed to play a role in repair of membrane wounds. Using a previously published approach (29), we monitored Ca^{2+}-dependent enlargeosome exocytosis by immunodetecting the cell surface appearance of the enlargeosomal marker AHNAK/desmoyokin. As for LAMP1, control and patient cells were wounded using glass beads in PBS with 2 mM $CaCl_2$ and 4 mg/mL FITC dextran. After allowing 5 min to heal, cells were immunostained for cell surface AHNAK. This marker was detected in 73 $\pm$ 9% of the wounded control fibroblasts ($n = 103$), but in a greater number of wounded cells from patient 1 (84 $\pm$ 7%; $n = 99$; $P = 0.04$) and patient 2 (89 $\pm$ 5%; $n = 89$; $P = 0.008$) (Figure 6A, B). However, a similar difference was observed between the number of unwounded patient and control cells that show cell surface AHNAK labeling [15% for control, 27% for patient 1 ($P = 0.0004$) and 28% for patient 2 ($P = 0.007$) (Figure 6C). Thus, the increased number of wounded patient cells with surface AHNAK may be due to higher basal, not calcium-triggered, cell surface translocation of AHNAK.

Discussion

Following identification of the role of dysferlin in MM, it has been recognized that not all forms of MM are linked to dysferlin mutations (30). For efficient diagnosis and treatment

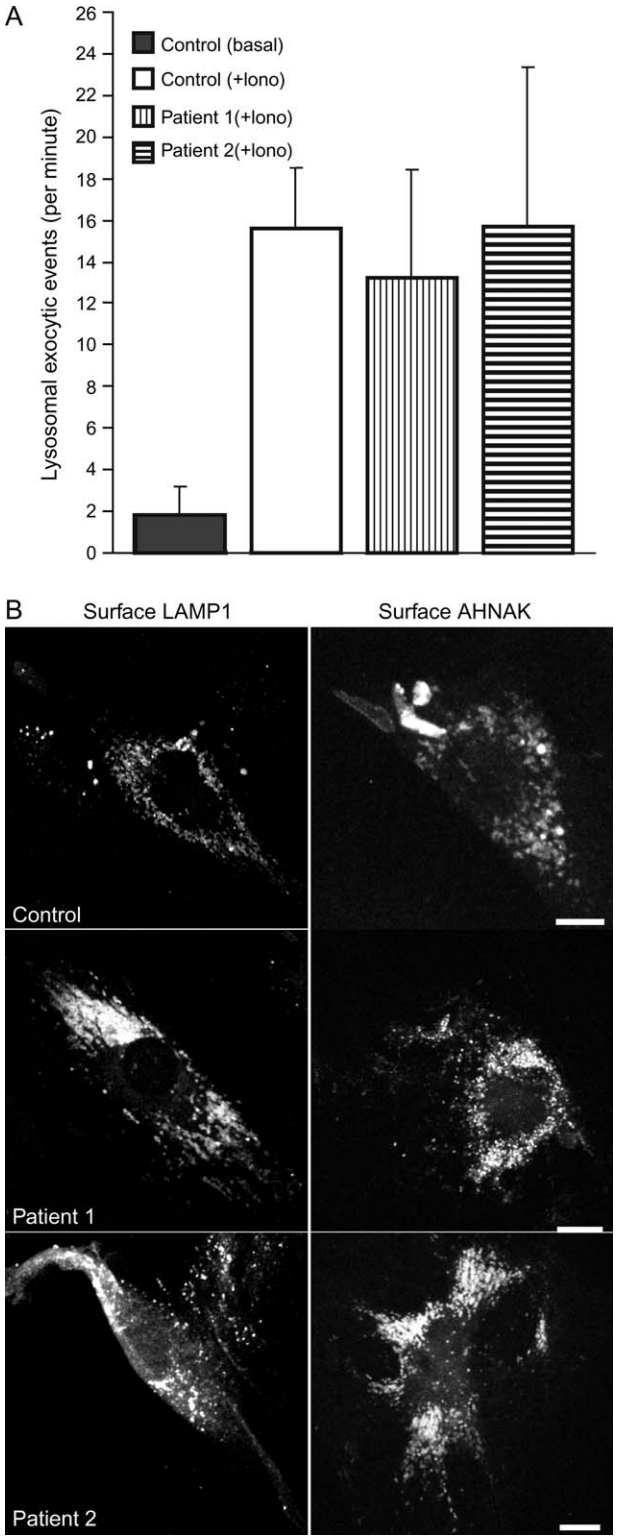

Figure 4: Calcium-triggers lysosomal and enlargeosomal exocytosis in patient cells. A) FITC dextran labeled lysosomes that exocytosed in the control and patient fibroblasts were monitored using TIR-FM (Videos S1–S3). The average of the number of lysosomes that exocytosed prior to ionophore addition (basal) or within a minute following the ionophore addition (+ iono) are shown. The results are an average of five (for +iono) or two (for basal) cells; the error bars show standard deviation. B) 10 μM calcium ionophore was added to cells in serum-free growth media. Ten minutes later, cell surface LAMP1 or AHNAK were labeled using H4A3 and KIS monoclonal antibodies, respectively. The cells were fixed and labeled with anti-mouse alexa 546 secondary antibody and nuclear stain Hoechst 3342. The images show 3D projection of 1-μm thick optical slices of individual LAMP1 and AHNAK-labeled cells imaged using 60 × 1.2 NA objective. Scale bar represents 10 μm.

of other forms of MM, it is important to understand their genetic and cellular basis. Despite the acknowledgments of genetic heterogeneity in MM, nothing is known regarding the pathomechanism(s) responsible for this muscular dystrophy. In this report, we provide evidence that poor ability to heal cell membrane wounds may be a common pathomechanism for MM-type muscular dystrophies. We analyzed cell membrane repair in a family with two patients who exhibit different clinical severity of the non-dysferlin MM phenotype. The cell membrane repair defects in these patients was established using two independent methods: (i) laser wounding, which allows monitoring the healing kinetics of individual cells; and (ii) bead wounding, which allows monitoring the proportion of wounded cells in a population that fail to heal. A smaller percentage of fibroblasts from the patient with severe non-dysferlin MM phenotype were able to heal. Moreover, those that did heal were slower at healing compared with healthy fibroblasts or those from the patient with milder MM phenotype. Thus, the extent of cell membrane resealing defect in these patients correlates with their serum CK levels and with the clinical severity of their disease. As the cells of patient 1 take longer to heal, this may explain why the serum CK level in this patient is much greater than the patient 2. Thus, these results suggest that poor membrane repair may be responsible for the muscular dystrophy in these patients.

Repair of membrane wound requires exocytosis of vesicles near or at the site of wounding, which is triggered by wound-mediated increase in intracellular calcium (20,21). This process appears to be present across all eukaryotic cells, however the precise mechanisms are still unclear. While the mechanism may vary between cell types in mammalian cells, at least two intracellular compartments, the lysosome and the enlargeosome, can fuse to the plasma membrane following Ca^{2+} elevation induced by a membrane injury (27,29). These compartments have been suggested to play a role in repair of membrane wounds; however, recent reports have contested the role of lysosomes in membrane repair (40,41). In dysferlinopathic muscle cells, lysosomal exocytosis is reported to be decreased (17). Based on this, a model has been proposed according to which dysferlin and annexin molecules aid in exocytosis of lysosomes, helping in the resealing of damaged sarcolemma (17). We found that cells from this

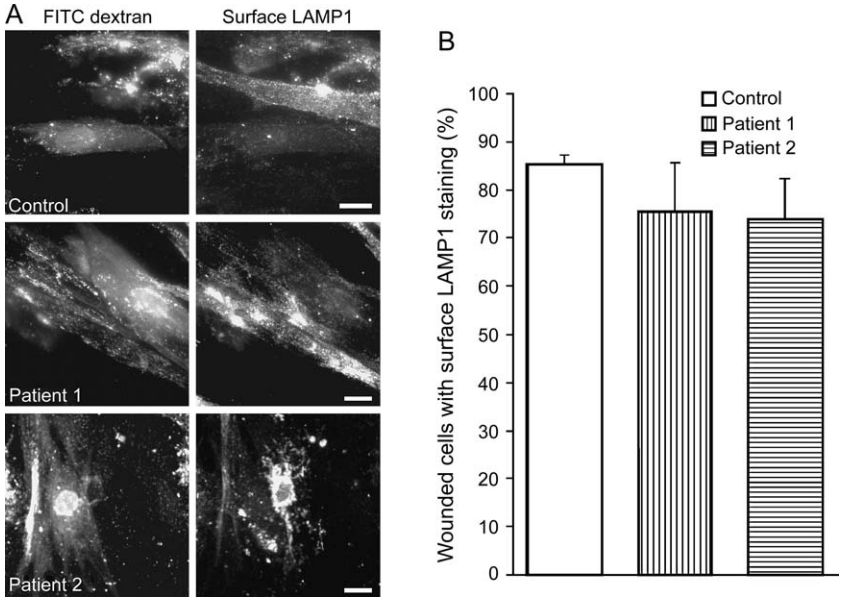

Figure 5: Plasma membrane wound induces exocytosis of lysosomes. Cells were wounded with glass beads in the presence of FITC dextran and cell surface LAMP1 and the nuclei were labeled as before. A) Epifluorescence images were acquired using a 20× 0.7 NA objective. Left panel shows dextran labeling and the right panel shows LAMP1 labeling, scale bar represents 10 μm. Note that as in Figure 3, cells that failed to heal (show low FITC fluorescence) are also the ones with most extensive lysosomal exocytosis. The cells that healed (have trapped most FITC dextran) have relatively less while the unwounded cells (unlabeled with FITC dextran) have almost no cell surface LAMP1 staining. LAMP1 labeling for each of these three types of cells is comparable between the control and the patient cells. B) Of the total wounded cells (>100 cells for each sample) in different region of the dish, cells that show cell surface LAMP1 staining were counted and their per cent fraction computed for each region. Error bars represent the SD values between these regions.

patient neither lack dysferlin nor annexin A2, and the calcium-triggered exocytosis of lysosome is unaltered. An alternate model for membrane repair has been proposed where dysferlin aids in exocytosis of dysferlin-containing vesicles which, it is suggested, aids in healing sarcolemmal membrane wounds (3). The identity of these dysferlin-containing vesicles is elusive, and there is no direct evidence if the dysferlin-containing vesicles or the lysosomes play a role in healing of wound in dysferlinopathic cells. As wounding-induced lysosome exocytosis is as efficient in the non-dysferlin MM patient cells as in the control cells, lack of lysosome exocytosis is not responsible for the membrane repair defect in these patients. A defect in the exocytosis of dysferlin-containing vesicles is still a possibility. If so, identification of the molecular defect in these cells would open the way for identifying the machinery involved in exocytosis of dysferlin-containing vesicles.

As we observed that wound healing in the patient cells is calcium dependent, the responsible compartment should be competent at calcium-triggered exocytosis. We have previously identified that in fibroblasts several intracellular compartments, including ER, Golgi, Golgi-derived vesicles and early endosomes, do not undergo calcium-triggered exocytosis (42). This narrows the list of potential compartments that could be responsible for this process in the patient cells. Recently, it has been proposed that preferential membrane trafficking from Golgi to the wound site may aid in healing cells that have been wounded once before (43). However, as these patient cells show poor healing even when wounded once, a post-Golgi vesicle trafficking defect may not be the cause for this defect. Thus, further analysis is needed to identify the compartment(s) and the mechanism(s) responsible for membrane repair defect in the non-dysferlin MM patient cells.

In a complimentary approach to identify the defects in the patient cells, we carried out a genetic analysis of the entire family in the hope of identifying the molecular basis of non-dysferlin MM in these patients. We examined the candidacy of several genes and chromosomal regions linked to dysferlin for their involvement in non-dysferlin MM. A strong candidate for this was the dysferlin-interacting protein caveolin-3. The caveolin-3 gene is mutated in several muscle diseases, including a distal muscular dystrophy and hyperCKemia. These diseases share similarities with non-dysferlin MM, including a leaky muscle cell membrane (32). Moreover, caveolin-3 localizes with dysferlin and is important for proper trafficking of dysferlin (31). Mutation screening revealed no pathogenic mutations in the patient's caveolin-3 gene. Due to its ability to interact with dysferlin in a calcium-dependent manner and its proposed role in aiding fusion of dysferlin-containing vesicles, annexin A2 has been suggested to be another

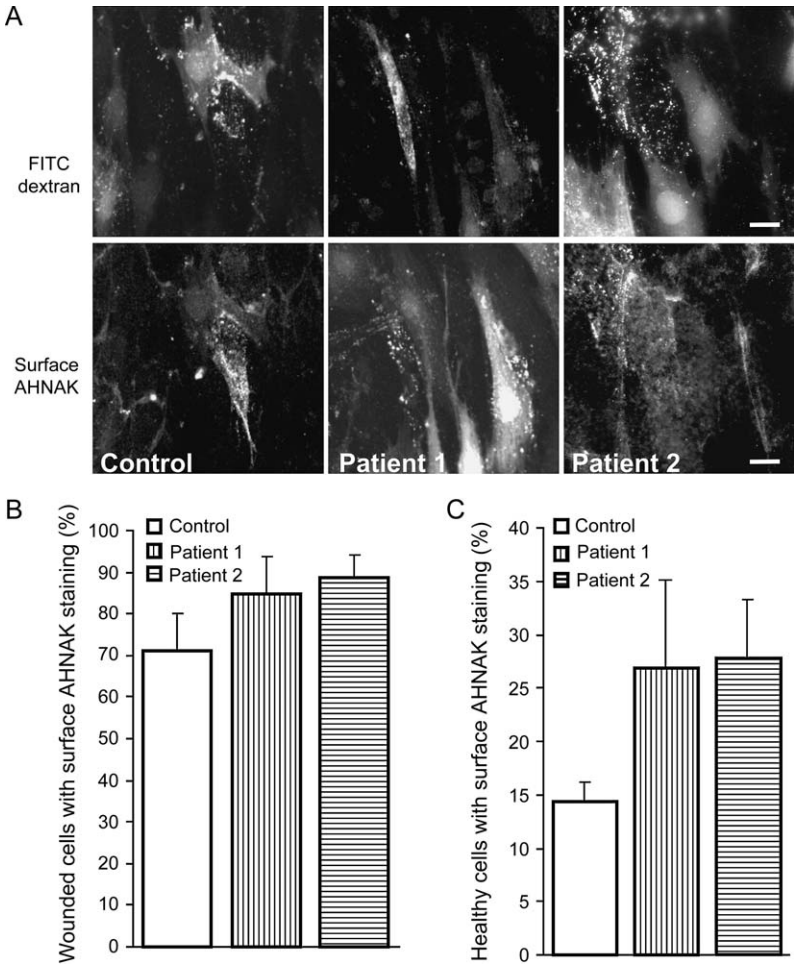

Figure 6: Plasma membrane wound induces exocytosis of enlargeosomes. Cells were wounded as above. After allowing cells to heal for 5 min, enlargeosomal exocytosis was monitored by immunolabeling cell surface AHNAK using KIS monoclonal antibody. A) Upper panel shows dextran labeling and the lower panel shows surface AHNAK labeling, scale bar represents 10 μm. B) Of the total wounded cells (>100 cells for each sample) in different region of the dish, cells that show cell surface AHNAK staining were counted and their per cent fraction was computed for each region. The plot shows the average values from these regions and the error bars represent the SD. C) Out of all the 100–300 healthy cells analyzed for each sample (from >5 regions in a dish), per cent fraction of cells showing cell surface AHNAK staining was computed for each region. The plot shows the average of values from these regions and the error bars represent the SD.

candidate for non-dysferlin MM. In both these patients, full-length annexin A2 is abundantly expressed, indicating that a lack or truncation of annexin A2 is not responsible for the disease in these patients. We also excluded lack of myoferlin expression and the involvement of the chromosome 10p region implicated in non-dysferlin MM, the MMD2 locus as the basis for this disease. Although our results highlight further genetic heterogeneity in non-dysferlin MM, this cannot be confirmed until the *MMD2* gene has been identified.

The observation that a non-dysferlin muscular dystrophy correlates with a failure in membrane repair highlights the importance of a common pathomechanism in dysferlin muscular dystrophy and non-dysferlin MM. Despite the identification of several dysferlin-interacting proteins, very little is known about the dysferlin membrane repair pathway. Our findings should help us to identify further families aiding us adopting a suitable genome analysis approach with the aim of identifying candidate genes and loci implicated in non-dysferlin MM. A concerted genetic and cell biological approach is now vital for to the identification of the gene(s) responsible for non-dysferlin MM. Identification of these genes may provide understanding of the dysferlin sarcolemmal repair pathway which is necessary for the development of therapies for these groups of muscular dystrophies.

Materials and Methods

Non-dysferlin MM families

Non-dysferlin MM families are identified on the basis of those showing a MM phenotype but displaying normal dysferlin protein expression and/or exclusion to the dysferlin locus by haplotype analysis. For the MM family described in this report, exclusion to dysferlin was obtained by dysferlin protein expression analysis. Skin fibroblast cultures were available from two affected patients and an age- and a gender-matched unrelated control individual. Informed consent was obtained from the patients and local ethical approval was obtained for the use of the DNA samples and the fibroblast cells.

Cell culture

Fibroblasts were cultured in F10-Ham media or DMEM (Invitrogen, Carlsbad, CA, USA) containing 20% FBS and 1% antibiotic (streptomycin and penicillin) in a humidified 37°C incubator with 5% CO2. C2C12 mouse myoblast cells were cultured similarly in DMEM with 10% FBS and 1% antibiotic. All experiments were carried out using cells between passages 1–6. For imaging, cells were plated on sterile coverslips (Fisher Scientific, Hampton, NH) 2–3 days prior to imaging. For monitoring lysosomal

exocytosis, lysosomes of the cells growing on coverslip were labeled with 70-kDa FITC dextran (Sigma-Aldrich, St. Louis, MO, USA) as previously described (42). For TIR-FM, coverslip was placed on the microscope stage in the Sykes Moore chamber (Bellco Glass, Vineland, NJ, USA), and cells were imaged in OptiMem media (Invitrogen) with 2 mM final calcium concentration. During imaging, calcium ionophore A23187 was added to the final concentration of 10 μM.

Membrane repair assays

Laser-mediated membrane wounding and analysis of resealing

The assay was performed on five fibroblasts from each patient in the presence of Ca^{2+} and three or more fibroblasts in the absence of Ca^{2+}. Cells were washed and kept in Dulbecco's PBS containing 1 mM Ca^{2+} for the resealing experiment in the presence of Ca^{2+} and in DPBS containing 1 mM EGTA for resealing experiment in the absence of Ca^{2+}. Cells were plated and kept at 37°C on a glass bottom plastic dish (MatTek, Ashland, MA, USA) and membrane damage was induced in the presence of 2 μM FM 1–43 dye (Molecular Probes Inc., Invitrogen, Eugene, OR, USA) with a femtosecond pulsed two-photon laser-scanning microscope (IR-Achroplan 40× 1.2 NA water immersion objective, LSM 510META; Carl Zeiss Inc., Thornwood, New York). To induce damage, a 5 μm × 5 μm area of the plasma membrane was irradiated at full power of 800 nm pulsed, mode-locked laser radiation from a 1-W Ti:Sapphire laser (Chameleon; Coherent Laser Group, Santa Clara, CA, USA). Cells were imaged at 10-seconds intervals by using 488 nm one-photon laser excitation. Imaging was started 20 seconds before to and continued for up to 7 min later. For every image, the fluorescence intensity at the site of the damage was measured with the Metamorph software (Molecular devices corporation, Sunnyvale, CA, USA).

Glass bead wounding and resealing assay

Patient and control fibroblasts were subjected to the following treatment. Cells grown on coverslips were transferred to PBS + 2 mM Ca^{2+} buffer containing 4 mg/mL lysine fixable 10-kDa FITC dextran. of Glass beads of about 40 mg (425–600 μm, Sigma) were sprinkled onto the cells and the beads were rolled gently 10–12 times over the cells to induce plasma membrane wounds. After wounding, the coverslips were incubated as such at 37°C for 5 min. Following two washes with dextran-free PBS + 2 mM Ca^{2+} buffer, cells were incubated with prewarmed PBS + 2 mM Ca^{2+} buffer containing 4 mg/mL lysine fixable 10-kDa TR dextran at 37°C for another 5-min period. The coverslips were then washed in PBS and fixed with 4% paraformaldehyde. The number of FITC-positive (total wounded cells) and TR-positive cells (wounded cells which have not resealed) were counted in 20 fields in duplicate. Cells were imaged using Olympus IX-70 inverted microscope with 60×, 1.2 NA water immersion objective and 525/50 nm and 560LP emission filters. The number of wounded cells that failed to reseal were expressed as a percentage of the total wounded cells.

TIR-FM

The TIR-FM illumination was set up as described previously (42). Total Internal Reflection was achieved using the objective setup (44) on an inverted fluorescence microscope (IX-70; Olympus) equipped with high numerical aperture lens (Apo 60× NA 1.45; Olympus). A custom-built temperature-controlled enclosure was used to maintain the microscope at 37°C during imaging. Cell labeled with FITC dextran were excited with the 488-nm line of Argon ion laser (Omnichrome, model 543-AP A01; Melles Griot, Carlsbad, CA). The depth of the evanescent field was typically 70–120 nm for the Apo 60× N.A. 1.45 lens (42,44). The emission was collected through emission band pass filter (HQ525/50M; Chroma Technologies Corp., Rockingham, VT, USA). Images were acquired at 5–10 frames/second using a 12-bit cooled CCD ORCA-ER (Hamamatsu Photonics, Bridgewater, NJ). The camera and mechanical shutters (Uniblitz; Vincent Associates, Rochester, NY) were controlled using MetaMorph (Molecular Devices, CA, USA).

Immunofluorescence imaging

To examine the fusion of lysosomes and enlargeosomes with the plasma membrane following glass-bead-mediated membrane wounding and re-sealing cell surface, LAMP1 and AHNAK were detected using the H4A3 LAMP1 antibody (27) (Developmental Studies Hybridoma Bank, University of Iowa, Iowa, IA, USA) and the KIS (45) AHNAK antibody, respectively. For this, cells were incubated with the appropriate antibody in 1% BSA (in PBS + 1 mM Ca^{2+}) at 4°C for 45 min followed by washing of the excess antibody and fixation of the cells with 4% paraformaldehyde solution. The cells were blocked again using 1% BSA and then stained with the appropriate fluorescently labeled secondary antibodies. Cells were imaged using Olympus IX-70 inverted microscope using 60×, 1.2 NA or 20×, 0.7 NA objective. The excitation and emission filters used are – 330-385BP:430-470BP for Hoechst, 450-490BP:500-550BP for FITC, 540-580BP:580LP for TR dextran and 450-490BP:560LP for Alexa 546 (Chroma Technologies Corp.).

Haplotype analysis

Microsatellite markers were used to generate haplotypes. Polymerase chain reaction (PCR) was performed using fluorescently labeled forward primer according to conditions described in UniSTS (http://www.ncbi.nlm.nih.gov/entrez/query.fcgi?db=unists). Following PCR, genotypes were generated using an ABI Prism 377XL DNA sequencer (Applied Biosystems, Foster City, CA, USA) using the software GeneScan® Analysis 3.1 (Applied Biosystems). Haplotypes were designated according to the length of the repeats. Haplotypes were generated for the following 10p microsatellite markers spanning the 10p region implicated in MMD2: tel-D10S1691-(2.1 Mb)-D10S1649 547-(4.6 Mb)-*D10S2325-(0.61 Mb)-D10S570-(1.37 Mb)-D10S1664-(0.26 Mb)-D10S191-(4.80 Mb)-D10S466-(3.38 Mb)-D10S1662-(7.56 Mb)-D10S1426-cen. To examine the dysferlin region, we analyzed the markers tel-D2S292- (0.086 Mb)-D2S443-(1.13 Mb)-*DYSF*-(0.02 Mb)-D2S291-(0.19 Mb)-D2S2977-(1.19 Mb)-D2S2111-cen. The physical distance between the markers was determined primarily through ENSEMBL (http://www.ensembl.org/Homo_sapiens/) except for the marker D10S2325, which had not been mapped in ENSEMBL. Its relative distance was determined using MapViewer (http://www.ncbi.nlm.nih.gov/mapview/maps.cgi).

DNA sequencing

Both exons of the *CAV3* gene were screened for mutations in both affected patient DNAs using intronic primers. The primers 5′ CTGCCACAGGAGGCTTTAGA 3′ and 5′ TCGCAAACCTGACACTCTCC 3′ were used to amplify exon 1 and 5′ CACACCCAAAAGCTTGAGAA 3′ and 5′ GCAGCCCCTGTGAAGAAGT 3′ for exon 2. The PCR products were sequenced using the BigDye Terminator v3.1 Cycle Sequencing Kit (Applied Biosystems) and electrophoresis was performed on the ABI PRISM 377XL DNA sequencer (Applied Biosystems). Sequencing data were collected using the ABI DNA Sequencing Analysis Software version 3.3 and analyzed with MegAlign version 4.05 (DNASTAR program).

Protein expression studies

Cells were homogenized in RIPA lysis buffer pH 7.4 (50 mM Tris HCl pH 7.4, 150 mM NaCl, 1% Triton-X-100, 1% sodium deoxycholate) with Complete Mini Protease Inhibitor cocktail (Roche Molecular Biochemicals, Mannheim, Germany) and centrifuged at 10 000× ***g*** at 4°C for 10 min. The protein concentrations of the extracted supernatant from the patient cells were determined using the Lowry method. Protein extracts (15 μg for dysferlin, annexin A2 and GAPDH and 31.5 μg for myoferlin) were separated on a 6–10% acrylamide gel and transferred to 0.45 μM nitrocellulose membrane (BDH, Heidelberg, Germany). Anti-dysferlin, anti-annexin A2 and anti-GAPDH antibodies were purchased commercially and used at dilutions of 1:100, 1:2000 and 1:1500 to 1:4000, respectively.

The monoclonal myoferlin antibody was generated to the myoferlin peptide C-GDEPPPERRDRDNDSDDVE where the first C was used to attach the carrier hemocyanin protein. This peptide represents amino acids 326–344 in myoferlin protein. The specificity of the monoclonal myoferlin antibody was confirmed by incubating the myoferlin antibody (1:50) with 100 μg/mL of

peptide overnight at 4°C prior to incubation with the blots containing 30 μg protein extracted from C2C12 myoblast cells. Monoclonal myoferlin antibody was used at a dilution of 1:50. Antibodies were incubated in 3–5% milk in 1× Tris buffered saline with 0.1–0.2% Tween-20. The secondary antibodies used were goat anti-mouse antibody conjugated to horseradish peroxidase (Jackson Immunoresearch, West Grove, PA, USA) diluted up to 1:10 000. Equal loading of protein on the blots was checked using the GAPDH antibody (1:1500).

Acknowledgments

We thank the non-dysferlin MM family members for all their co-operation in this study. The monoclonal myoferlin antibody was generated and gifted to R. B. by the late Louise Anderson and Arun Deora provided help with the Western blot analysis of annexin A2. Support by the Rockefeller University Bioimaging facility and Alison North's help with laser wounding assay is acknowledged. We thank Josh Rappoport for comments on the manuscript. This work was supported by grants from the Muscular Dystrophy Campaign UK to R. B. J. K. J. and S. M. S. acknowledge grants from NSF (BES-0119468 and BES-0322867) and NIH (1P20GM072015-01).

Supplementary Materials

Video 1: Lysosomal exocytosis in control cells. Lysosomes of control fibroblasts growing on glass coverslip were labeled with FITC dextran. Cells were imaged by TIR-FM using 60× 1.45 NA objective and 488-nm laser excitation. Video shows a single cell imaged at six frames per second and the elapsed time is shown at the top right corner of the video. During imaging, cells were treated with 10 μM ionomycin, which resulted in exocytosis of lysosomes. As described previously (42), each exocytic event appears as the flash of FITC dextran fluorescence, which is caused by diffusion of the FITC dextran in the extracellular space away from the site of fusion.

Video 2: Lysosomal exocytosis in cells from patient 1. Lysosomes in fibroblasts of patient 1 were labeled with FITC dextran and imaged by TIR-FM as for the control fibroblasts. Video shows a single cell imaged at five frames per second and the elapsed time is shown at the top right corner of the video. During imaging, cells were treated with 10 μM ionomycin causing lysosomes to exocytose. Individual exocytic event appears as a flash of FITC dextran fluorescence, which is due to the diffusion of the FITC dextran in the extracellular space away from the site of fusion.

Video 3: Lysosomal exocytosis in cells from patient 2. Lysosomes in fibroblasts of patient 2 were labeled with FITC dextran and imaged by TIR-FM as for the control fibroblasts. Video shows a single cell imaged at five frames per second and the elapsed time is shown at the top right corner of the video. Lysosomal exocytosis was triggered during imaging by treating cells with 10 μM ionomycin. Each exocytic event appears as a flash of FITC dextran fluorescence, which is due to the diffusion of the FITC dextran in the extracellular space away from the site of fusion.

Supplemental materials are available as part of the online article at http://www.blackwell-synergy.com

References

1. Cohn RD, Campbell KP. Molecular basis of muscular dystrophies. Muscle Nerve 2000;23:1456–1471.
2. Bushby KM. The limb-girdle muscular dystrophies-multiple genes, multiple mechanisms. Hum Mol Genet 1999;8:1875–1882.
3. Bansal D, Campbell KP. Dysferlin and the plasma membrane repair in muscular dystrophy. Trends Cell Biol 2004;14:206–213.
4. Anderson LV, Davison K, Moss JA, Young C, Cullen MJ, Walsh J, Johnson MA, Bashir R, Britton S, Keers S, Argov Z, Mahjneh I, Fougerousse F, Beckmann JS, Bushby KM. Dysferlin is a plasma membrane protein and is expressed early in human development. Hum Mol Genet 1999;8:855–861.
5. Matsuda C, Aoki M, Hayashi YK, Ho MF, Arahata K, Brown RH Jr. Dysferlin is a surface membrane-associated protein that is absent in Miyoshi myopathy. Neurology 1999;53:1119–1122.
6. Piccolo F, Moore SA, Ford GC, Campbell KP. Intracellular accumulation and reduced sarcolemmal expression of dysferlin in limb – girdle muscular dystrophies. Ann Neurol 2000;48:902–912.
7. Illarioshkin SN, Ivanova-Smolenskaya IA, Greenberg CR, Nylen E, Sukhorukov VS, Poleshchuk VV, Markova ED, Wrogemann K. Identical dysferlin mutation in limb-girdle muscular dystrophy type 2B and distal myopathy. Neurology 2000;55:1931–1933.
8. Bashir R, Britton S, Strachan T, Keers S, Vafiadaki E, Lako M, Richard I, Marchand S, Bourg N, Argov Z, Sadeh M, Mahjneh I, Marconi G, Passos-Bueno MR, Moreira Ede S et al. A gene related to Caenorhabditis elegans spermatogenesis factor fer-1 is mutated in limb-girdle muscular dystrophy type 2B. Nat Genet 1998;20:37–42.
9. Liu J, Aoki M, Illa I, Wu C, Fardeau M, Angelini C, Serrano C, Urtizberea JA, Hentati F, Hamida MB, Bohlega S, Culper EJ, Amato AA, Bossie K, Oeltjen et al. Dysferlin, a novel skeletal muscle gene, is mutated in Miyoshi myopathy and limb girdle muscular dystrophy. Nat Genet 1998;20:31–36.
10. Achanzar WE, Ward S. A nematode gene required for sperm vesicle fusion. J Cell Sci 1997;110:1073–1081.
11. Yasunaga S, Grati M, Cohen-Salmon M, El Amraoui A, Mustapha M, Salem N, El Zir E, Loiselet J, Petit C. A mutation in OTOF, encoding otoferlin, a FER-1-like protein, causes DFNB9, a nonsyndromic form of deafness. Nat Genet 1999;21:363–369.
12. Davis DB, Delmonte AJ, Ly CT, McNally EM. Myoferlin, a candidate gene and potential modifier of muscular dystrophy. Hum Mol Genet 2000;9:217–226.
13. Britton S, Freeman T, Vafiadaki E, Keers S, Harrison R, Bushby K, Bashir R. The third human FER-1-like protein is highly similar to dysferlin. Genomics 2000;68:313–321.
14. Doherty KR, McNally EM. Repairing the tears: dysferlin in muscle membrane repair. Trends Mol Med 2003;9:327–330.
15. Yasunaga S, Grati M, Chardenoux S, Smith TN, Friedman TB, Lalwani AK, Wilcox ER, Petit C. OTOF encodes multiple long and short isoforms: genetic evidence that the long ones underlie recessive deafness DFNB9. Am J Hum Genet 2000;67:591–600.
16. Bansal D, Miyake K, Vogel SS, Groh S, Chen CC, Williamson R, McNeil PL, Campbell KP. Defective membrane repair in dysferlin-deficient muscular dystrophy. Nature 2003;423:168–172.
17. Lennon NJ, Kho A, Bacskai BJ, Perlmutter SL, Hyman BT, Brown RH Jr. Dysferlin interacts with annexins A1 and A2 and mediates sarcolemmal wound-healing. J Biol Chem 2003;278:50466–50473.
18. Straub V, Rafael JA, Chamberlain JS, Campbell KP. Animal models for muscular dystrophy show different patterns of sarcolemmal disruption. J Cell Bio 1997;139:375–385.
19. Selcen D, Stilling G, Engel AG. The earliest pathologic alterations in dysferlinopathy. Neurology 2001;56:1472–1481.
20. McNeil PL, Steinhardt RA. Plasma membrane disruption: repair, prevention, adaptation. Annu Rev Cell Dev Biol 2003;19:697–731.
21. Steinhardt RA, Bi G, Alderton JM. Cell membrane resealing by a vesicular mechanism similar to neurotransmitter release. Science 1994; 263:390–393.
22. Sudhof TC. Synaptotagmins: why so many? J Biol Chem 2002;277: 7629–7632.

23. Sudhof TC, Rizo J. Synaptotagmins: C2-domain proteins that regulate membrane traffic. Neuron 1996;17:379–388.
24. Chapman ER. Synaptotagmin: a Ca(2+) sensor that triggers exocytosis? Nat Rev Mol Cell Biol 2002;3:498–508.
25. Schiavo G, Osborne SL, Sgouros JG. Synaptotagmins: more isoforms than functions? Biochem Biophys Res Commun 1998;248:1–8.
26. Davis DB, Doherty KR, Delmonte AJ, McNally EM. Calcium-sensitive phospholipid binding properties of normal and mutant ferlin C2 domains. J Biol Chem 2002;277:22883–22888.
27. Reddy A, Caler EV, Andrews NW. Plasma membrane repair is mediated by Ca(2+)-regulated exocytosis of lysosomes. Cell 2001;106:157–169.
28. Ampong BN, Imamura M, Matsumiya T, Yoshida M, Takeda S. Intracellular localization of dysferlin and its association with the dihydropyridine receptor. Acta Myol 2005;24:134–144.
29. Borgonovo B, Cocucci E, Racchetti G, Podini P, Bachi A, Meldolesi J. Regulated exocytosis: a novel, widely expressed system. Nat Cell Biol 2002;4:955–962.
30. Linssen WH, de Visser M, Notermans NC, Vreyling JP, Van Doorn PA, Wokke JH, Baas F, Bolhuis PA. Genetic heterogeneity in Miyoshi-type distal muscular dystrophy. Neuromuscul Disord 1998;8:317–320.
31. Hernandez-Deviez DJ, Martin S, Laval SH, Lo HP, Cooper ST, North KN, Bushby K, Parton RG. Aberrant dysferlin trafficking in cells lacking caveolin or expressing dystrophy mutants of caveolin-3. Hum Mol Genet 2006;15:129–142.
32. Woodman SE, Sotgia F, Galbiati F, Minetti C, Lisanti MP. Caveolinopathies: mutations in caveolin-3 cause four distinct autosomal dominant muscle diseases. Neurology 2004;62:538–543.
33. Doherty KR, Cave A, Davis DB, Delmonte AJ, Posey A, Earley JU, Hadhazy M, McNally EM. Normal myoblast fusion requires myoferlin. Development 2005;132:5565–5575.
34. Nishino I, Malicdan MC, Murayama K, Nonaka I, Hayashi YK, Noguchi S. Molecular pathomechanism of distal myopathy with rimmed vacuoles. Acta Myol 2005;24:80–83.
35. Vajsar J, Zhang W, Dobyns W B, Biggar D, Holden K R, Hawkins C, Ray P, Olney A H, Burson C M, Srivastava A K, Schachter H. Carriers and patients with muscle-eye-brain disease can be rapidly diagnosed by enzymatic analysis of fibroblasts and lymphoblasts. Neuromuscul Disord 2006;16:132–136.
36. Higashi K, Higuchi I, Niiyama T, Uchida Y, Shiraishi T, Hashiguchi A, Saito A, Horikiri T, Suehara M, Arimura K, Osame M. Abnormal expression of proteoglycans in Ullrich's disease with collagen VI deficiency. Muscle Nerve 2006;33:120–126.
37. Lammerding J, Hsiao J, Schulze PC, Kozlov S, Stewart CL, Lee RT. Abnormal nuclear shape and impaired mechanotransduction in emerin-deficient cells. J Cell Biol 2005;170:781–791.
38. Muchir A, Medioni J, Laluc M, Massart C, Arimura T, van der Kooi AJ, Desguerre I, Mayer M, Ferrer X, Briault S, Hirano M, Worman HJ, Mallet A, Wehnert M, Schwartz K et al. Nuclear envelope alterations in fibroblasts from patients with muscular dystrophy, cardiomyopathy, and partial lipodystrophy carrying lamin A/C gene mutations. Muscle Nerve 2004;30:444–450.
39. Jaiswal JK, Chakrabarti S, Andrews NW, Simon SM. Synaptotagmin VII restricts fusion pore expansion during lysosomal exocytosis. Plos Biology 2004;2:1224–1232.
40. Cerny J, Feng Y, Yu A, Miyake K, Borgonovo B, Klumperman J, Meldolesi J, McNeil PL, Kirchhausen T. The small chemical vacuolin-1 inhibits Ca(2+)-dependent lysosomal exocytosis but not cell resealing. EMBO Rep 2004;5:883–888.
41. Shen SS, Tucker WC, Chapman ER, Steinhardt RA. Molecular regulation of membrane resealing in 3T3 fibroblasts. J Biol Chem 2005; 280:1652–1660.
42. Jaiswal JK, Andrews NW, Simon SM. Membrane proximal lysosomes are the major vesicles responsible for calcium-dependent exocytosis in nonsecretory cells. J Cell Biol 2002;159:625–635.
43. Togo T. Disruption of the plasma membrane stimulates rearrangement of microtubules and lipid traffic toward the wound site. J Cell Sci 2006;119:2780–2786.
44. Jaiswal JK, Simon SM. Total internal reflection fluorescence microscopy for high resolution imaging of cell surface events. Current Protocols in Cell Biology (Bonifacino JS, Dasso M, Lippincott-Schwartz J, Harford JB, and Yamada KM, eds) John Wiley and Sons Inc., New Jersey, 2003; 4.12.1–4.12.15.
45. Hohaus A, Person V, Behlke J, Schaper J, Morano I, Haase H. The carboxyl-terminal region of ahnak provides a link between cardiac L-type Ca2+ channels and the actin-based cytoskeleton. FASEB J 2002;16:1205–1216.